



Molecular dynamics analysis on bending mechanical behavior of alumina nanowires at different loading rates

Yuxiao James HE¹, Bin MA²

1. School of Materials Science and Engineering, Tsinghua University, Beijing 100084, China;

2. School of Architecture and Traffic Engineering, Guilin University of Electronic Technology, Guilin 541004, China

Received 29 January 2022; accepted 2 June 2022

Abstract: The molecular dynamics (MD) model of α -Al₂O₃ nanowires in bending is established by using LAMMPS to calculate the atomic stress and strain at different loading rates in order to study the effect of loading rate on the bending mechanical behaviors of the α -Al₂O₃ nanowires. Research results show that the maximum surface stress–rotation angle curves of α -Al₂O₃ nanowires at different loading rates are all divided into three stages of elastic deformation, plastic deformation and failure, where the elastic limit point can be determined by the curve symmetry during loading and unloading cycle. The loading rate has great influence on the plastic deformation but little on the elastic modulus of α -Al₂O₃ nanowires. When the loading rate is increased, the plastic deformation stage is shortened and the material is easier to fail in brittle fracture. Therefore, the elastic limit and the strength limit (determined by the direct and indirect MD simulation methods) are closer to each other. The MD simulation result of α -Al₂O₃ nanowires is verified to be valid by the good agreement with the improved loop test results. The direct MD method becomes an effective way to determine the elastic limit and the strength limit of nanoscale whiskers failed in brittle or ductile fracture at arbitrary loading rate.

Key words: alumina nanowires; bending behavior; loading rate; elastic limit; strength limit; molecular dynamics

1 Introduction

In recent years, one-dimensional nanostructure oxides have attracted more and more attention of researchers because of their excellent properties in optics, magnetism, superconductivity and ferroelectricity [1–3]. As one of the important nanostructure materials, alumina nanowires have wide application prospects in composite reinforcement and nano-devices, owing to its good mechanical and optical properties [4,5], and high thermal and chemical stability [6]. Currently, the study of alumina nanowires is focused on its tensile mechanical properties [7,8] and little on its bending mechanical properties [9–11]. It is of great significance to study the bending strength and

deformation mechanism of alumina nanowires, not only for ensuring the safety and stability of alumina nanowires but also for expanding their application range in engineering [12,13].

In theoretical study, classical or modified Euler Bernoulli beam theory was used to calculate the bending mechanical properties of one-dimensional nanostructures [9,10,14], but its accuracy and applicability in nano scale needed to be verified. In experimental study, although the cantilever bending method [9] and three-point bending method [10,15] based on atomic force microscope (AFM) were adopted to measure the bending mechanical properties of alumina nanowires, the sliding and friction between the sample and AFM tip would result in significant measurement errors [11]. Loop test, by twisting a loop in a fiber and pulling the

fiber ends until the loop breaks, was originally proposed to measure the fracture strain and strength of optical fibers [16]. Now, it has been widely used to measure the strength of various fiber materials [17,18], since the strain and strength can be determined by simply measuring the diameter and width of the ring at fracture, and the measurement range was confined within a small area (in the neighborhood of the looped-fiber apex instead of along the whole length) to avoid the weakest defects or microcracks in the measured fibers [16,17]. A modified loop test was developed by WANG et al [11] to measure the bending strength of alumina nanowires in good agreement with the theoretical results. However, there is still lack of study on the bending deformation micro-mechanism.

Considering the limitations of experimental conditions and testing technology, computational simulation method based on atomic level has undoubtedly become the most effective way to study the mechanical properties and deformation mechanism of nanowires. The molecular dynamics method has been widely used to reveal the internal deformation mechanism of nanostructured materials by calculating the evolution process of atomic motion [19–21]. Currently, available literatures are mainly related to the bending deformation and mechanical properties of one-dimensional metal nanowires based on molecular dynamics method, e.g., cantilever bending deformation [22], three-point bending deformation [23–25] and four-point bending deformation [26], but little to the bending deformation mechanism of metal oxide nanowires. Furthermore, the effect of loading rate on the

bending deformation of one-dimensional nanostructures is less studied.

In this study, bending mechanical behavior of α -Al₂O₃ nanowires (as a typical example of metal oxide nanowires) at different loading rates was studied by the molecular dynamics (MD) simulation method. Firstly, the MD model of α -Al₂O₃ nanowires in bending was established by using LAMMPS to calculate the atomic stress and strain at different loading rates based on the virial stress theorem and local transformation matrix. Then, the effect of loading rate on the bending mechanical behaviors of α -Al₂O₃ nanowires was analyzed in detail, including the maximum surface stress–rotation angle curves, bending deformation mechanism, elastic limit and strength limit. Finally, a modified loop test of α -Al₂O₃ whiskers was adopted to verify the validity and reliability of the MD calculation model and simulation results.

2 Calculation model and method

2.1 Calculation model

Figure 1 shows the schematic diagram of calculation model and loading form for α -Al₂O₃ nanowires in bending, where the basic cell model is hexagonal cell (Fig. 1(a)) with lattice parameters: $a=b=4.759$ Å, $c=12.991$ Å, $\alpha=\beta=90^\circ$, $\gamma=120^\circ$. The large-scale cell structure was first established by extending the basic cell in space and then cut into the required nano whisker model, a long cube of 80 nm \times 3 nm \times 3 nm with square section (Fig. 1(b)). The bending moment was applied by fixing the atoms of central region b (1 nm \times 3 nm \times 3 nm) and rotating a pair of rigid end-regions a and

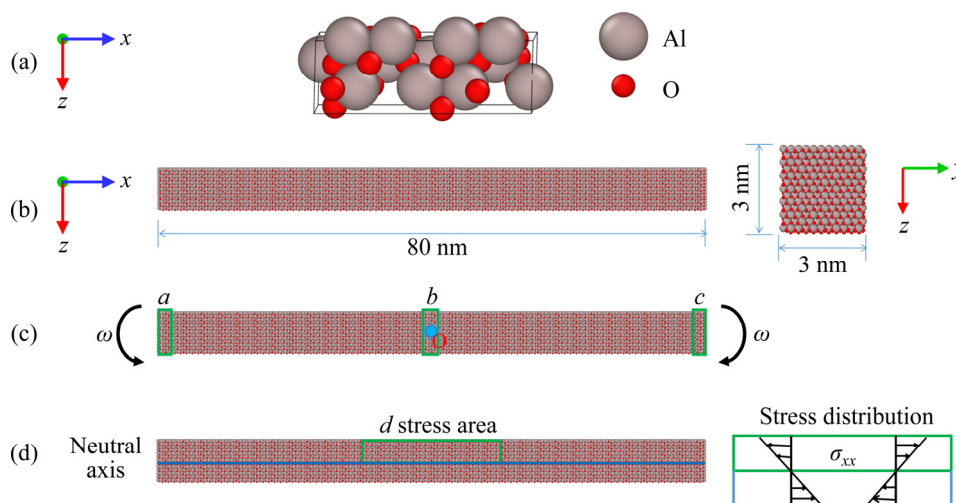


Fig. 1 Schematic diagram of calculation model and loading form

c ($1 \text{ nm} \times 3 \text{ nm} \times 3 \text{ nm}$) about the rotation center point o (Fig. 1(c)) at a constant rotational angular velocities ω ($\omega=0.006, 0.009, 0.012, 0.015, 0.018$ ($^\circ$)/ps). The bending deformation mechanism of the α -Al₂O₃ nanowires can be analyzed by simulating the average stress of all atoms in the central region d ($20 \text{ nm} \times 3 \text{ nm} \times 1.5 \text{ nm}$) varying with the loading time (Fig. 1(d)).

2.2 Calculation method

In order to study the bending mechanical behaviors of α -Al₂O₃ nanowires, it is necessary to firstly define the atomic stress as the intensity component of atomic interaction, which can be calculated by EAM potential function equation as follows [27]:

$$\sigma_{\alpha}^{ij} = \frac{1}{\Omega_{\alpha}} \{-m_{\alpha} v_{\alpha}^i v_{\alpha}^j + \frac{1}{2} \sum_{\beta \neq \alpha} \left[\frac{\partial \phi}{\partial r_{\alpha\beta}} + \left(\frac{\partial F}{\partial \rho_{\alpha}} + \frac{\partial F}{\partial \rho_{\beta}} \right) \frac{\partial f}{\partial r_{\alpha\beta}} \right] \frac{r_{\alpha\beta}^i r_{\alpha\beta}^j}{r_{\alpha\beta}} \} \quad (1)$$

where σ_{α}^{ij} , Ω_{α} , m_{α} and v_{α} are stress tensor component, volume, mass and velocity component of the atom α , respectively; ϕ , F , ρ_{α} , ρ_{β} , $r_{\alpha\beta}$ and f are parameters of EAM potential function equation.

The average atomic stress $\bar{\sigma}$ of the material can be obtained by solving the average value of the local stress σ for all atoms ($\alpha=1, 2, \dots, N$) [28]:

$$\bar{\sigma} = \frac{1}{N} \sum_{\alpha=1}^N \sigma(\alpha) \quad (2)$$

According to the continuum elasticity theory, the normal stress on the cross section of one-dimensional nanostructure still approximately obeys the linear distribution in bending deformation (Fig. 1(d)) [12,23]. Thus, the maximum normal stress of bending surface can be defined as

$$\sigma_{\max} = 2\bar{\sigma} \quad (3)$$

When the large-scale parallel computing software LAMMPS is adopted in molecular dynamics simulation, selection of the potential function is very important for the accuracy of calculation results. Based on the charge transfer potential of ion solid (proposed by STREITZ and MINTMIRE [29]) and the metal alloy embedded atom method (for solving the interaction between metals and ions), ZHOU et al [30] proposed a new embedded atom potential function of the metal

alloys and their oxides to successfully predict the surface relaxation and electric-charge variation in different regions of multilayer system, e.g., on the free surface of metal oxide, inside the body of metal alloy and metal oxide, and on the metal/metal oxide interface.

In this study, the new embedded atomic potential function of metal oxide was adopted for molecular dynamics simulation of α -Al₂O₃ nanowires by using LAMMPS, where the boundary conditions were set as the free boundary in X and Y directions and the periodic boundary in X direction. The temperature was controlled at 0.01 K with isothermal adjustment by Nose–Hoover method for eliminating the influence of thermal activation in the calculation. For the MD simulation calculation, the specimen of α -Al₂O₃ nanowires was firstly subjected to molecular dynamics relaxation at 0.01 K with a time step of 2 fs in order to ensure the lowest and stable system energy. Then, it was simulated in bending under the NVT ensemble until the material was damaged. Finally, the atomic stress and strain could be calculated based on the virial stress theorem and local transformation matrix [31,32] in order to further calculate the maximum normal stress of bending surface by Eqs. (1)–(3).

3 Results and analyses

3.1 Maximum surface stress–rotation angle curves at different loading rates

Figure 2 shows the maximum surface stress of α -Al₂O₃ nanowires varying with the total rotation angle at different loading rates ($\omega=0.006, 0.009, 0.012, 0.015, 0.018$ ($^\circ$)/ps). All of these curves are divided into three stages: elastic deformation stage ($OO_1, OP_1, OQ_1, OR_1, OS_1$) with very little change of slope, plastic deformation stage ($O_1O_2, O_1P_2, O_1Q_2, O_1R_2, O_1S_2$) and failure stage ($O_2O_3, O_2P_3, O_2Q_3, O_2R_3, O_2S_3$). For the sake of clarity, Fig. 3 gives the maximum surface stress–rotation angle curve and the energy–time curve of α -Al₂O₃ nanowires under $\omega=0.006$ ($^\circ$)/ps as an example. It is seen that the potential energy–time curve (Fig. 3(b)) also has three stages: $OO_I, O_I O_{II}$ and $O_{II} O_{III}$, corresponding to the elastic deformation (OO_I), plastic deformation ($O_I O_2$) and failure ($O_2 O_3$) in the maximum surface stress–rotation angle curve (Fig. 3(a)), respectively. The kinetic energy is almost

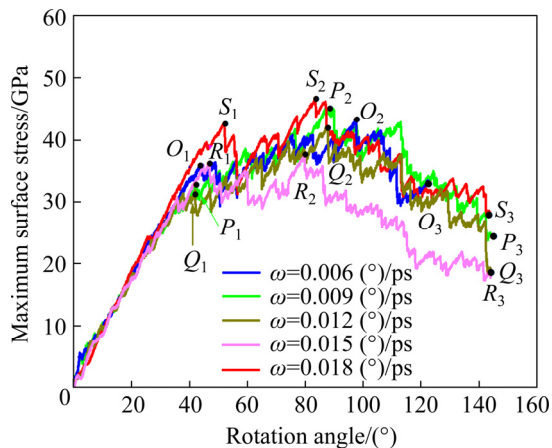


Fig. 2 Maximum surface stress of α -Al₂O₃ nanowires varying with total rotation angle at different loading rates

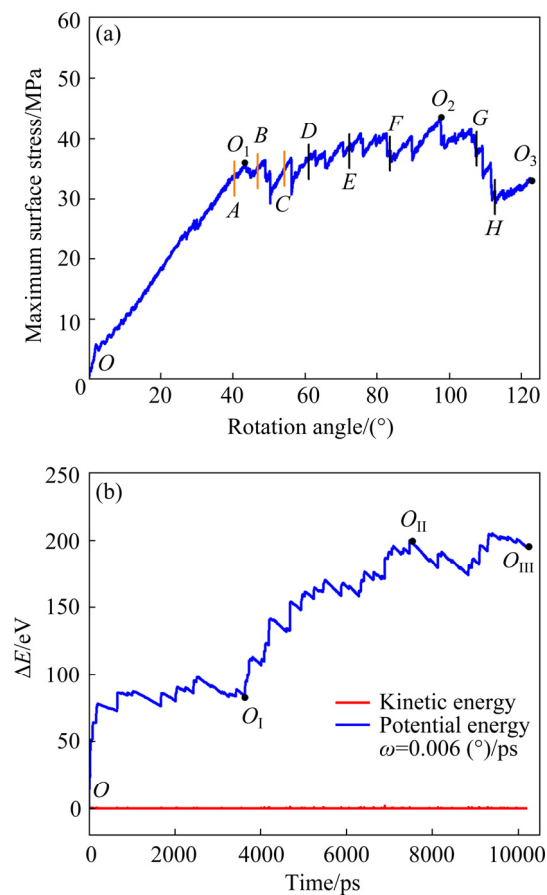


Fig. 3 Maximum surface stress–rotation angle curve (a) and energy–time curve (b) of α -Al₂O₃ nanowires ($\omega=0.006$ (°)/ps)

equal to zero independent of the loading time, indicating that the angular velocity ($\omega=0.006$ (°)/ps) provides a quasi-static loading.

In order to further prove that the point O_1 represents the bending elastic limit of α -Al₂O₃ nanowires, two points A_1 (38.4°, 3200 ps) and B_1

(48°, 4000 ps) near the point O_1 (43.2°, 3600 ps) are selected to simulate and analyze the loading–unloading effect on the maximum surface stress (Fig. 4). When the α -Al₂O₃ nanowires are loaded to the point A_1 before the plastic deformation and then unloaded from the point A_1 to the point A_2 , the maximum surface stress is reduced to zero and the recovered angle (i.e., $76.8^\circ-38.4^\circ$) from the point A_1 (38.4°) to A_2 (76.8°) is equal to the original angle of point A_1 (38.4°). The loading (OA_1) and unloading (A_1A_2) curves have identical slopes and appear to be symmetrical, which reflects the full elastic recovery of the α -Al₂O₃ nanowires at the point A_1 .

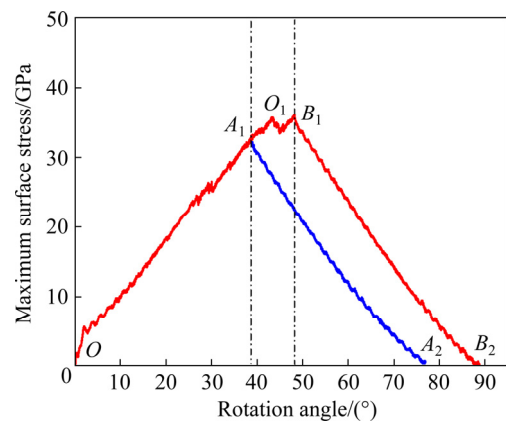


Fig. 4 Maximum surface stress–rotation angle curve of α -Al₂O₃ nanowires ($\omega=0.006$ (°)/ps) during loading and unloading cycle

When the α -Al₂O₃ nanowires are loaded to the point B_1 (48°, 4000 ps) after the elastic deformation and then unloaded from the point B_1 to the point B_2 (88.8°, 7400 ps), the maximum surface stress is reduced to zero but the recovered angle (i.e., $88.8^\circ-48^\circ$) from the point B_2 (88.8°) to the point B_1 (48°) is smaller than the original angle of point B_1 (48°), i.e., with a residual angle of 7.2°. In this case, the loading (OB_1) and unloading (B_1B_2) curves are no longer symmetrical, indicating the permanent plastic deformation of the α -Al₂O₃ nanowires at the point B_1 . Therefore, the bending elastic limit of α -Al₂O₃ nanowires can be determined by the stress of the point O_1 .

3.2 Bending deformation mechanism at different loading rates

3.2.1 Bending deformation evolution process

As an example, the bending deformation evolution process of the α -Al₂O₃ nanowires at

$\omega=0.006$ ($^{\circ}$)/ps is analyzed in detail as follows, where the atomic shear strain is often used to characterize the plastic deformation of nano-materials [33].

(1) Elastic deformation stage (O_1O_2)

Three points *A*, *B* and *C* near the limit point O_1 of elastic deformation (Fig. 3(a)) are selected for analyzing the microstructures and shear strains of the α -Al₂O₃ nanowires (Fig. 5), where their bending angles (loading times) are 38.4° (3200 ps), 48° (4000 ps) and 54° (4500 ps), respectively. It is seen that when the loading time is 3200 ps (Fig. 5(a)), there appears obvious bending deformation of microstructures with very small shear strain (all of atom region is almost in dark-blue). When the loading time is increased to 4000 ps (Fig. 5(b)) and 4500 ps (Fig. 5(c)), the α -Al₂O₃ nanowires continue to bend and light-colored atoms (large shear strain) are observed in the central region. Furthermore, the light-colored atom region tends to increase with the increasing of the loading time. This means that the α -Al₂O₃ nanowires undergo the elastic deformation at the point *A* (the point O_1 is the bending elastic limit), and start to be damaged at points *B* and *C*.

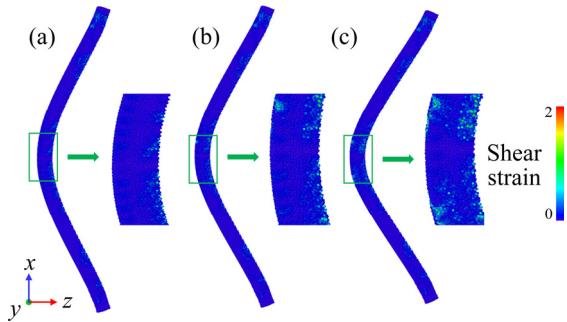


Fig. 5 Microstructures and shear strain distributions of α -Al₂O₃ nanowire ($\omega=0.006$ ($^{\circ}$)/ps) at different loading time (near point O_1): (a) 3200 ps; (b) 4000 ps; (c) 4500 ps

(2) Plastic deformation stage (O_1O_2)

Three points *D*, *E* and *F* in the stage O_1O_2 (Fig. 3(a)) are selected for analyzing the microstructures and shear strains of the α -Al₂O₃ nanowires (Fig. 6), where their bending angles (loading times) are 60° (5000 ps), 72° (6000 ps) and 84° (7000 ps), respectively. It is seen that when the loading time is 5000 ps (Fig. 6(a)), the number of light-colored atoms (large shear strain) is larger than that at 4500 ps (Fig. 5(c)) in the central region of α -Al₂O₃ nanowires. When the loading time is increased to 6000 ps (Fig. 6(b)) and 7000 ps

(Fig. 6(c)), the α -Al₂O₃ nanowires continue to bend, with the appearing of more light-colored atoms (large shear strain) and the red-colored atoms (higher shear strain) in the central region. However, no crack is found in the α -Al₂O₃ nanowires, indicating that the stage O_1O_2 is only in plastic deformation without any fracturing.

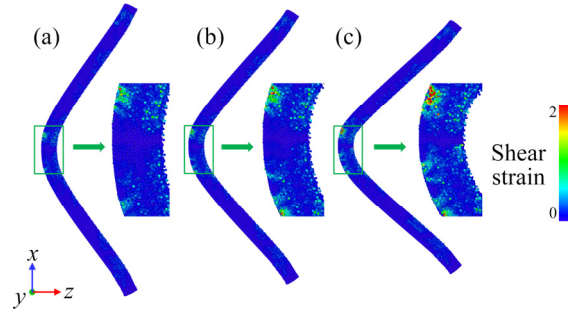


Fig. 6 Microstructures and shear strain distributions of α -Al₂O₃ nanowires ($\omega=0.006$ ($^{\circ}$)/ps) at different loading time (in O_1O_2 stage): (a) 5000 ps; (b) 6000 ps; (c) 7000 ps

(3) Failure stage (O_2O_3)

Two points *G* and *H* in the failure stage O_2O_3 (Fig. 3(a)) are selected for analyzing the microstructures and shear strains of the α -Al₂O₃ nanowires (Fig. 7), where their bending angles (loading times) are 108° (9000 ps) and 120° (10000 ps), respectively. It is seen that when the loading time is 9000 ps (Fig. 7(a)), local cracking appears near the red atoms in the central area of α -Al₂O₃ nanowires. When the loading time is increased to 10000 ps (Fig. 7(b)), both the red atoms (higher shear strain) and the cracking area are gradually increased, leading to the final failure of α -Al₂O₃ nanowires (stage O_2O_3).

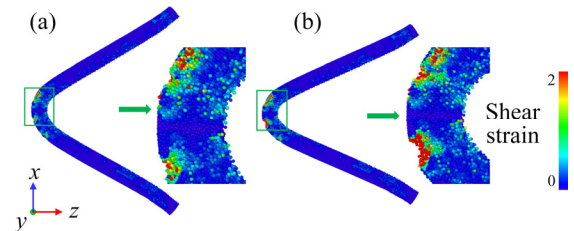


Fig. 7 Microstructures and shear strain distributions of α -Al₂O₃ nanowires ($\omega=0.006$ ($^{\circ}$)/ps) at different loading time (in O_2O_3 stage): (a) 9000 ps; (b) 10000 ps

3.2.2 Effect of loading rates

Figures 8 and 9 show the bending deformation curvatures of α -Al₂O₃ nanowires at the elastic limit

points (O_1, P_1, Q_1, R_1, S_1) and the strength limit points (O_2, P_2, Q_2, R_2, S_2) at different loading rates. Obviously, the former is much larger than the latter. They are both little changed when $\omega \leq 0.015$ ($^\circ$)/ps, but greatly increased (i.e., the curvature radii are greatly decreased) when $\omega = 0.018$ ($^\circ$)/ps. Detail values of the bending curvature radii at different loading rates are listed in Table 1. Therefore, the effect of loading rate on the bending deformation curvatures of α -Al₂O₃ nanowires must be taken into account when the loading rate is relatively high.

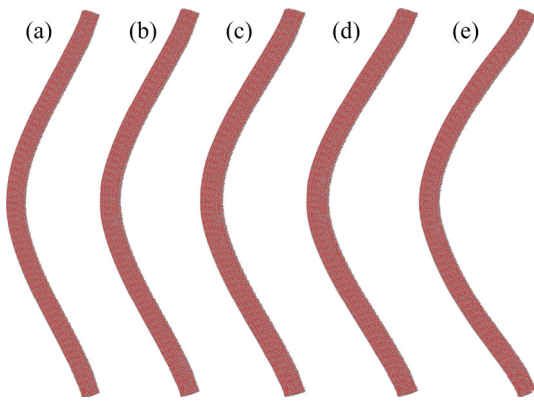


Fig. 8 Bending deformation curvatures of α -Al₂O₃ nanowires at elastic limit points (O_1, P_1, Q_1, R_1, S_1) under different loading rates: (a) 0.006 ($^\circ$)/ps; (b) 0.009 ($^\circ$)/ps; (c) 0.012 ($^\circ$)/ps; (d) 0.015 ($^\circ$)/ps; (e) 0.018 ($^\circ$)/ps

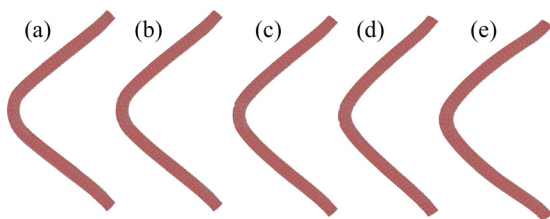


Fig. 9 Bending deformation curvatures of α -Al₂O₃ nanowires at strength limit points (O_1, P_1, Q_1, R_1, S_1) under different loading rates: (a) 0.006 ($^\circ$)/ps; (b) 0.009 ($^\circ$)/ps; (c) 0.012 ($^\circ$)/ps; (d) 0.015 ($^\circ$)/ps; (e) 0.018 ($^\circ$)/ps

Table 1 Minimum curvature radii of bending deformation for elastic limit and strength limit of α -Al₂O₃ nanowires at different loading rates

ω [$^\circ \cdot \text{ps}^{-1}$]	$(R_e)_{\min}/\text{\AA}$	$(R_b)_{\min}/\text{\AA}$
0.006	232.07	168.37
0.009	231.3	173.05
0.012	230.37	179.98
0.015	228.64	184.35
0.018	193.4	154.6

Figure 10 shows the microstructures and shear strain distributions of the α -Al₂O₃ nanowires under the same loading displacement of failure stage (i.e., at the same rotation angle of 120 $^\circ$) at different loading rates. Obviously, under the same loading displacement, the larger the loading rate is, the larger the cracking area is, indicating that the failure form of α -Al₂O₃ nanowires is gradually changed from plasticity to brittleness.

3.3 Elastic limit and strength limit at different loading rates

As shown in Fig. 11(a), when the loading rate is small (i.e., $\omega < 0.015$ ($^\circ$)/ps), the bending elastic limit and the strength limit of α -Al₂O₃ nanowires

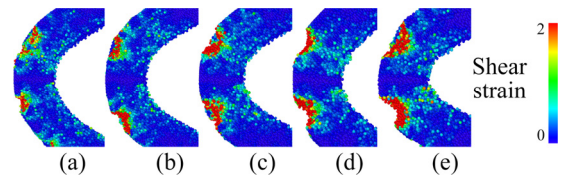


Fig. 10 Microstructures and shear strain distributions of α -Al₂O₃ nanowires at same rotation angle (120 $^\circ$) under different loading rates: (a) 0.006 ($^\circ$)/ps; (b) 0.009 ($^\circ$)/ps; (c) 0.012 ($^\circ$)/ps; (d) 0.015 ($^\circ$)/ps; (e) 0.018 ($^\circ$)/ps

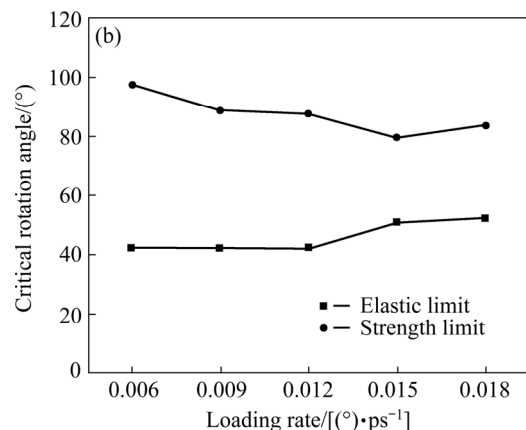
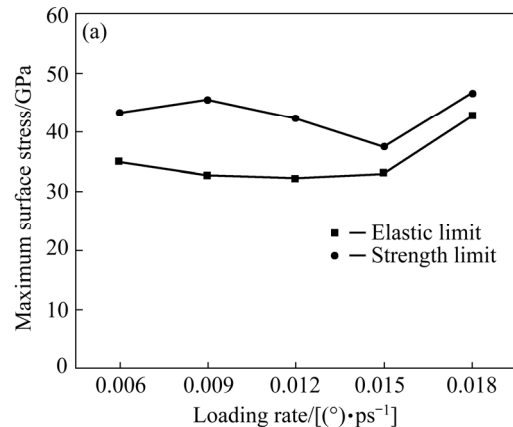


Fig. 11 Limit stresses (a) and critical rotation angles (b) of α -Al₂O₃ nanowires varying with loading rate

are slightly changed as a whole. Both of them are greatly increased when the loading rate is large (i.e., $\omega > 0.015$ (°)/ps) and gradually tend to be equal. With the increasing of loading rate (Fig. 11(b)), the critical rotation angle of the elastic limit point is gradually increased, while that of the strength limit is gradually decreased. They also tend to be equal finally. Obviously, the larger the loading rate is, the closer to each other the elastic limit and strength limit is and the smaller the plastic deformation stage is, which indicates again that the α -Al₂O₃ nanowire material is changed gradually from plasticity to brittleness when the loading rate is increased.

4 Test verification

4.1 Improved loop test for α -Al₂O₃ whiskers in bending

(1) Test arrangement

An improved loop test for experimentally approaching the intrinsic strength of α -Al₂O₃ whiskers [11] was adopted to verify the validity of simulation results. The α -Al₂O₃ whisker was twisted into a loop on the substrate of SiN TEM grid by an electrochemically etched tungsten tip at a speed of

200 nm/s, under high-magnification optical microscopy attached to the scanning laser Doppler vibrometer (LDV, Polytec MSA-500 with an optic lens of Mitutoyo M Plan APO 100×). During bending, the adhesion and the static friction between the substrate and whisker loop were sufficiently strong to prevent the loop from untwisting and recoiling even after the pulling force was released. When the whisker loop was characterized by SEM (JEOL 7001 operated at 5 keV) or by TEM (Philips Tecnai F20 operated at 200 keV) and then removed from the SEM/TEM chamber, it could be further pulled into a smaller loop and re-imaged by SEM/TEM. The above-mentioned process was repeated until the whisker loop fractured into two segments, which were then characterized by SEM/TEM to examine their fracture behaviors.

(2) Test results

Figure 12 shows the loop test for α -Al₂O₃ whiskers, where Figs. 12(a–c) show the three optical images of the intermediate bending state, just before and immediately after fracture of the whisker loop, respectively. It is seen that the α -Al₂O₃ whisker loop before fracture (Fig. 12(b)) has the same shape as the theoretical loop

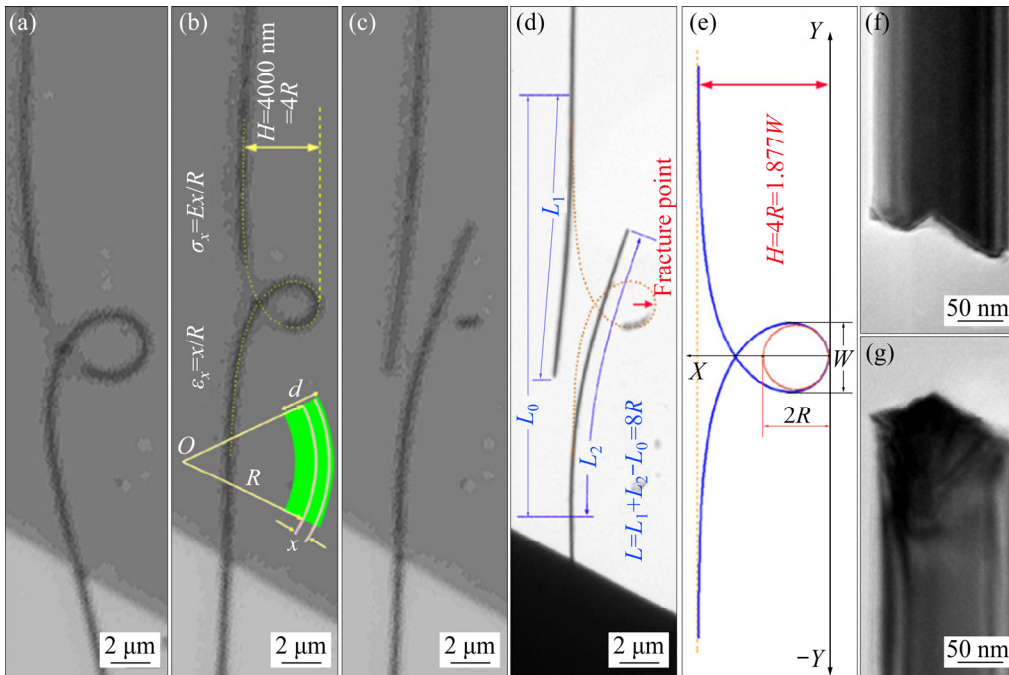


Fig. 12 Loop test for α -Al₂O₃ whiskers: (a–c) Three optical images showing intermediate bending state, just before and immediately after fracture, respectively; (d) TEM image corresponding to (c) with arrow showing fracture point of loop; (e) Theoretical loop shape based on classical elastic theory [16]; (f, g) High-magnification TEM images of two fractures in (d) (The yellow dotted curves in (b) and (d) indicate the theoretical shape [11])

(Fig. 12(e)) based on classical elastic theory [16], indicating that the whisker is deformed elastically until failure. Moreover, the fracture point of the whisker loop occurring near the bending apex (Fig. 12(d)) and the two whisker segments with V-shaped and faceted fracture ends (Figs. 12(f, g)) could prove that the fracture of the α -Al₂O₃ whisker loop is brittle.

For an elastically bent whisker, the strain ε_x and the stress σ_x at a distance x from the neutral axis can be expressed as $\varepsilon_x=x/R$ and $\sigma_x=xE/R$ based on classical elastic theory [34], where R is the radius of the inscribed circle of the neutral axis and E is the elastic modulus of the nanowires. Therefore, the maximum tensile strain ε_{\max} (fracture strain) and the maximum tensile stress σ_{\max} (fracture strength) on the outermost edge of the bending apex can be written as

$$\varepsilon_{\max}=d/(2R_{\min}), R_{\min}=L/8, \sigma_{\max}=E\varepsilon_{\max} \quad (4)$$

where d is the diameter of the α -Al₂O₃ whiskers and L is the overlap length between the two segments (Fig. 12(d)) [16].

The loop tests of 14 α -Al₂O₃ whiskers were conducted, in which the diameter d ranged from 82 to 320 nm, and $E=460$ GPa [11]. According to the measured values of L by using TEM (Fig. 12(d)) and Eq. (4), one can obtain the fracture strain ε_{\max} ($\varepsilon_{\max}=6.1\%–10.6\%$, with an average strain of 8.5%) and the corresponding fracture strength σ_{\max} ($\sigma_{\max}=28.1–48.8$ GPa, with an average strength of 39.1 GPa).

4.2 Comparison of simulation results with test results

4.2.1 Indirect MD simulation method for determining elastic limit and strength limit

As shown in Fig. 11(a), the elastic limit and strength limit of α -Al₂O₃ nanowires at different loading rates can be directly obtained by the maximum surface stress–rotation angle curves at different loading rates (Fig. 2), which is named as the direct molecular dynamics (MD) simulation method. In addition, there is another indirect MD simulation method for determining the limit stresses of α -Al₂O₃ nanowires based on classical elastic theory (Eq. (4)) as follows.

In MD simulation results, there exist two minimum curvature radii of α -Al₂O₃ nanowires,

$(R_e)_{\min}$ and $(R_b)_{\min}$, which correspond to the elastic limit (σ_e) and the strength limit (σ_b), respectively. As an example, Fig. 13 shows $(R_e)_{\min}$ and $(R_b)_{\min}$ of the bending deformation curve corresponding to σ_e (at the point O_1 , Fig. 2) and σ_b (at the point O_2 , Fig. 2), when the loading rate (rotation angular velocity) ω is 0.006 (°)/ps. Besides, Table 1 lists the fitting results of $(R_e)_{\min}$ and $(R_b)_{\min}$ for the α -Al₂O₃ nanowires at different loading rates. Therefore, by substituting these values of $(R_e)_{\min}$ and $(R_b)_{\min}$ as well as the diameter and elastic modulus of α -Al₂O₃ whiskers ($d=30$ Å, $E=460$ GPa [11]) into Eq. (4), one can obtain the elastic limit σ_e^* and strength limit σ_b^* of the α -Al₂O₃ nanowires, as listed in Table 2.

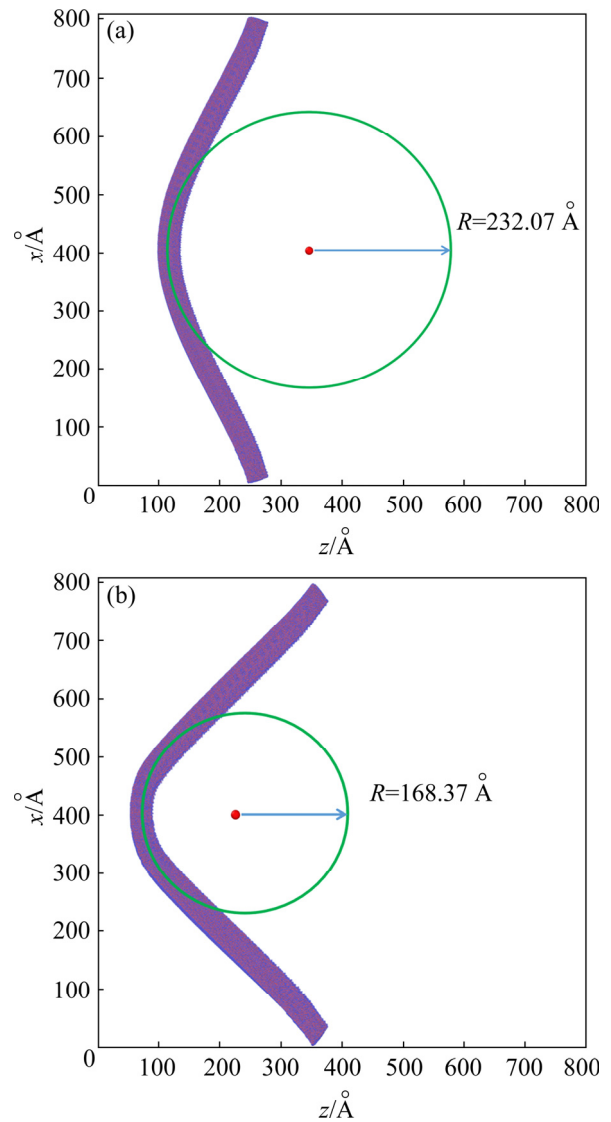


Fig. 13 Minimum bending curvature radius of α -Al₂O₃ nanowires corresponding to elastic limit and strength limit ($\omega=0.006$ (°)/ps): (a) $(R_e)_{\min}$ at point O_1 ; (b) $(R_e)_{\min}$ at point O_2

Table 2 Simulation results of elastic limit and strength limit by direction and indirect MD methods for α -Al₂O₃ nanowires at different loading rates as well as test results for comparison

Parameter	Simulation result					Test result
	$\omega=0.006$ (°)/ps	$\omega=0.009$ (°)/ps	$\omega=0.012$ (°)/ps	$\omega=0.015$ (°)/ps	$\omega=0.018$ (°)/ps	
σ_e /GPa	34.90	32.60	32.07	32.96	42.69	–
σ_e^* /GPa	29.70	29.83	29.95	30.18	35.68	–
σ_b /GPa	43.38	45.46	42.35	37.49	46.55	–
σ_b^* /GPa	40.98	39.87	38.34	37.43	44.60	28.10–48.80 (Average σ_b^* 39.10)

*—Obtained by Eq. (4) (i.e., indirect MD simulation method)

4.2.2 Comparison of strength limits obtained by different MD methods and experimental method

Figure 14 illustrates the elastic limit and strength limit of the α -Al₂O₃ nanowires obtained by the direct and indirect MD simulation methods varying with the loading rate (ω). It is seen that the elastic limits, σ_e and σ_e^* , are little changed when $\omega \leq 0.015$ (°)/ps and increased greatly when $\omega > 0.015$ (°)/ps. Besides, the strength limits, σ_b and σ_b^* , are slightly increased when $\omega < 0.015$ (°)/ps, but increased greatly and almost identical when $\omega \geq 0.015$ (°)/ps. It is concluded that the loading rate has great influence on the bending plastic deformation of α -Al₂O₃ nanowire but little on elastic modulus (Fig. 2). The larger the loading rate is, the shorter the plastic deformation stage is, the more easily the material tends to fail in brittle fracture and thus the closer the elastic limit to the strength limit is. Obviously, it can be found from Table 2 that, at the higher loading rate ω ($=0.015$ and 0.018 (°)/ps), the strength limit σ_b (37.49 and 46.55 GPa) obtained by the MD simulated curve (Fig. 2) with smaller plastic deformation is approximately equal to the strength limit σ_b^* (37.30 and 47.60 GPa) obtained by the classical elastic theory (Eq. (4)) regardless of plastic deformation. Besides, the strength limit σ_b^* (37.30 and 47.60 GPa) is closer to elastic limit σ_e (32.96 and 42.69 GPa) under the higher loading rate ω ($=0.015$ and 0.018 (°)/ps). This can prove again that the higher loading rate results in the higher brittleness of α -Al₂O₃ nanowires with smaller plastic deformation and thus the elastic limit is very closer to the strength limit.

Furthermore, it is also found from Table 2 that, the simulation results of the strength limit σ_b^* (37.43–44.60 MPa) is very close to the test result

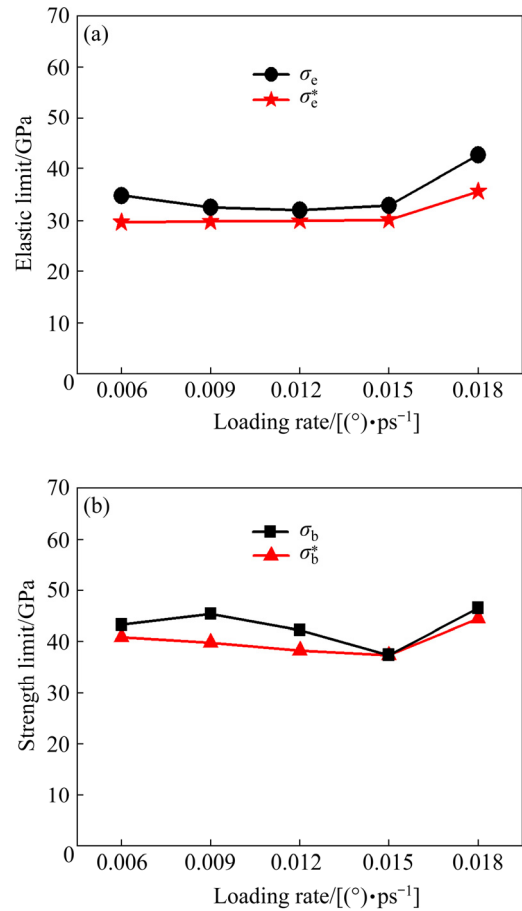


Fig. 14 Elastic limit and strength limit of α -Al₂O₃ nanowires obtained by direct and indirect MD simulation methods varying with loading rate: (a) Elastic limit (σ_e and σ_e^*); (b) Strength limit (σ_b and σ_b^*)

of average strength limit (39.10 GPa), which can verify the validity and reliability of this MD calculation model and simulation results. Since the α -Al₂O₃ nanowire is considered as the homogeneous and continuous material in the MD simulation calculation, while the real α -Al₂O₃ whiskers used in the loop inevitably have micro defects, the simulation result is a little higher than the test result.

It is worth noting that the improved loop test is based on the classic elasticity theory and thus only applicable for measuring the intrinsic bending strength of nanoscale whiskers failed in brittle fracture (regardless of plastic deformation). The direct MD simulation method is a better way to determine the elastic limit and strength limit of the nanoscale whiskers no matter what kind of failure form and loading rate are.

5 Conclusions

(1) The molecular dynamics model of α -Al₂O₃ nanowires in bending is established by using LAMMPS to calculate the atomic stress and strain at different loading rates based on the virial stress theorem and local transformation matrix. The effect of loading rate on the bending mechanical behaviors of α -Al₂O₃ nanowires is analyzed in detail, including the maximum surface stress–rotation angle curve, bending deformation mechanism, elastic limit and strength limit.

(2) The maximum surface stress–rotation angle curves of α -Al₂O₃ nanowires at different loading rates are all divided into three stages of elastic deformation (with very little change of slope), plastic deformation and failure. The elastic limit can be determined by the curve symmetry during loading and unloading cycle. The potential energy varying with the time also presents three similar stages of elastic deformation, plastic deformation and failure, while the kinetic energy varying with the time reflects the state of loading rate (static, quasi-static and dynamic loading).

(3) The bending deformation curvatures of α -Al₂O₃ nanowire at the elastic limit points and the strength limit points at different loading rates are both little changed when the loading rate is relatively small, but greatly increased when the loading rate is large. The larger the loading rate is, the larger the cracking area is, and the failure form of α -Al₂O₃ nanowires is gradually changed from plasticity to brittleness.

(4) The loading rate has great influence on the plastic deformation but little on the elastic modulus of α -Al₂O₃ nanowire. The larger the loading rate is, the shorter the plastic deformation stage is and the more easily the material tends to fail in brittle fracture. Therefore, the elastic limit and the strength limit (both determined by the direct and indirect

MD simulation methods) are closer to each other.

(5) The MD simulation results of α -Al₂O₃ nanowires are verified to be valid by the good agreement with the improved loop test results. Since the improved loop test is based on the classic elasticity theory, it is only applicable for measuring the intrinsic bending strength of nanoscale whiskers failed in brittle fracture (regardless of plastic deformation). The direct MD method becomes an effective way to determine the elastic limit and the strength limit of nanoscale whiskers failed in brittle or ductile fracture at arbitrary loading rate.

Acknowledgments

The work was supported by the National Natural Science Foundation of China (No. 12162010), the Science Technology Base and Talent Special Project of Guangxi, China (No. AD19245143), and Natural Science Foundation of Guangxi, China (No. 2021GXNSFAA220087).

References

- [1] KAJLI S K, RAY D, ROY S C. Efficient UV–visible photodetector based on single CuO/Cu₂O core–shell nanowire [J]. *Journal of Alloys and Compounds*, 2022, 895: 162546.
- [2] DAOUDI K, GAIDI M, COLUMBUS S, SHAMEER M, ALAWADHI H. Hierarchically assembled silver nanoprism–graphene oxide–silicon nanowire arrays for ultrasensitive surface enhanced Raman spectroscopy sensing of atrazine [J]. *Materials Science in Semiconductor Processing*, 2022, 138: 106288.
- [3] CHANG Y Q, WANG D B, LUO X H, XU X Y, CHEN X H, LI L, CHEN C P, WANG R M, XU J, YU D P. Synthesis, optical, and magnetic properties of diluted magnetic semiconductor Zn_{1-x}Mn_xO nanowires via vapor phase growth [J]. *Applied Physics Letters*, 2003, 83(19): 4020–4022.
- [4] DRAGIC P, CAVILLON M, BALLATO J. The linear and nonlinear refractive index of amorphous Al₂O₃ deduced from aluminosilicate optical fibers [J]. *International Journal of Applied Glass Science*, 2018, 9(3): 421–427.
- [5] SATYANARAYANA R S, LOKESHA H S, NAGABHUSHANA K R. Fabrication of spectroscopic characterization techniques using an optical fiber-based spectrometer [J]. *Review of Scientific Instruments*, 2021, 92: 093104.
- [6] ZUBASHCHENKO R V. Heat-insulating properties of high-alumina materials filament-reinforced with glass fiber of the Al₂O₃–SiO₂ and Al₂O₃–SiO₂–ZrO₂ systems [J]. *Refractories and Industrial Ceramics*, 2019, 59: 552–554.
- [7] SONG Xiao-lei, ZHANG Ke-chao, SONG Ying, DUAN Zhen-xin, LIU Qiang, LIU Yang. Morphology, microstructure and mechanical properties of electrospun alumina

- nanofibers prepared using different polymer templates: A comparative study [J]. *Journal of Alloys and Compounds*, 2020, 829: 154502.
- [8] CHOUDHARY K, LIANG T, CHERNATYNSKIY A, PHILLPOT S R, SINNOTT S B. Charge optimized many-body (COMB) potential for Al_2O_3 materials, interfaces, and nanostructures [J]. *Journal of Physics Condensed Matter*, 2015, 27: 305004.
- [9] VAHTRUS M, UMALAS M, POLYAKOV B, DOROGIN L, SAAR R, TAMME M, SAAL K, LOHMUS R, VLASSOV S. Mechanical and structural characterizations of gamma- and alpha-alumina nanofibers [J]. *Materials Characterization*, 2015, 107: 119–124.
- [10] WANG Yi, ZHANG Ao, LI Guang-de, LIU Shao-peng, XIANG Yang, CHENG Hai-feng. Sintering temperature and interphase effects on mechanical properties of an oxide fiber-reinforced Al_2O_3 - SiO_2 composite fabricated by sol-gel method [J]. *Applied Composite Materials*, 2021, 28: 321–339.
- [11] WANG Shi-liang, HE Yue-hui, HUANG Han, ZOU Jin, AUCHTERLONIE G J, HOU Li-zhen, HUANG Bai-yun. An improved loop test for experimentally approaching the intrinsic strength of alumina nanoscale whiskers [J]. *Nanotechnology*, 2013, 24(28): 285703.
- [12] ZHU Wen-peng, WANG Hong-tao, YANG Wei. Orientation- and microstructure-dependent deformation in metal nanowires under bending [J]. *Acta Materialia*, 2012, 60(20): 7112–7122.
- [13] ZHU Cheng-xin, CAO Feng, XIANG Yang, PENG Zhi-hang. Thermal shock resistance of $\text{Al}_2\text{O}_3/\text{SiO}_2$ composites by sol-gel [J]. *Ceramics International*, 2019, 45: 11270–11274.
- [14] ZHANG S B. Microstructure and surface orientation-dependent mechanical behaviors of Ag nanowires under bending [J]. *Computational Materials Science*, 2014, 95: 53–62.
- [15] ZHAO Zhi-hua, SHEN Xiao-qing, YAO Hong-chang, WANG Jian-she, CHEN Jin-zhou, LI Zhong-jun. Alumina nanofibers obtained via electrospinning of pseudo-boehmite sol/PVP solution [J]. *Journal Sol-Gel Science and Technology*, 2014, 70(1): 72–80.
- [16] SINCLAIR D. A bending method for measurement of the tensile strength and Young's modulus of glass fibers [J]. *Journal Applied Physics*, 1950, 21(5): 380–386.
- [17] MATTHEWSON M J, KURKJIAN C R, GULATI S T. Strength measurement of optical fibers by bending [J]. *Journal of the American Ceramic Society*, 1986, 69: 815–821.
- [18] FUKUDA H, YAKUSHIJI M, WADA A. A loop test to measure the strength of monofilaments used for advanced composites [J]. *Advanced Composite Materials*, 1999, 8: 281–291.
- [19] LIU Xiang-jun, ZHOU Hang-bo, ZHANG Gang, ZHANG Yong-wei. The effects of curvature on the thermal conduction of bent silicon nanowire [J]. *Journal of Applied Physics*, 2019, 125: 082505.
- [20] XIAO Qi-xin, HOU Zhao-yang, LI Chang, NIU Yuan. Mechanical property and deformation mechanism of gold nanowire with non-uniform distribution of twinned boundaries: A molecular dynamics simulation study [J]. *Chinese Physics B*, 2021, 30(5): 056101.
- [21] EGHBALIAN M, ANSARI R, HAGHIGHI S. Molecular dynamics study of mechanical properties and fracture behavior of carbon and silicon carbide nanotubes under chemical adsorption of atoms [J]. *Diamond and Related Materials*, 2022, 121: 108764.
- [22] VLASSOV S, METS M, POLYAKOV B, BIAN Jian-jun, DOROGIN L, ZADIN V. Abrupt elastic-to-plastic transition in pentagonal nanowires under bending [J]. *Beilstein Journal of Nanotechnology*, 2019, 10: 2468–2476.
- [23] NOHRING W G, MOLLER J J, XIE Zhuo-cheng, BITZEK E. Wedge-shaped twins and pseudoelasticity in fcc metallic nanowires under bending [J]. *Extreme Mechanics Letters*, 2016, 8: 140–150.
- [24] REDDY K V, PAL S. Influence of dislocations, twins, and stacking faults on the fracture behavior of nanocrystalline Ni nanowire under constant bending load: A molecular dynamics study [J]. *Journal of Molecular Modeling*, 2018, 24: 277.
- [25] KATAKAM K C, YEDLA N. Influence of orientation and temperature on the mechanical properties and deformation behavior of nickel nanowire under bending: A large scale molecular dynamics simulation [J]. *Materials Today: Proceedings*, 2021, 39: 1727–1732.
- [26] WANG Zhi-jia, LIU Chong, LI Zhi-gang, ZHANG Tong-yi. Size-dependent elastic properties of Au nanowires under bending and tension-Surfaces versus core nonlinearity [J]. *Journal of Applied Physics*, 2010, 108: 083506.
- [27] WU H A. Molecular dynamics study of the mechanics of metal nanowires at finite temperature [J]. *European Journal Mechanics-A/Solids*, 2006, 25(2): 370–377.
- [28] KOH S J A, LEE H P. Molecular dynamics simulation of size and strain rate dependent mechanical response of FCC metallic nanowires [J]. *Nanotechnology*, 2006, 17: 3451–3467.
- [29] STREITZ F H, MINTMIRE J W. Electrostatic potentials for metal-oxide surfaces and interfaces [J]. *Physical Review B*, 1994, 50(16): 11996–12003.
- [30] ZHOU X W, WADLEY H N G, FILHOL J S, NEUROCK M N. Modified charge transfer-embedded atom method potential for metal/metal oxide systems [J]. *Physical Review B*, 2004, 69: 035402.
- [31] FALK M L, LANGER J S. Dynamics of viscoplastic deformation in amorphous solids [J]. *Physical Review E*, 1998, 57(6): 7192–7205.
- [32] SHIMIZU F, OGATA S, LI J. Theory of shear banding in metallic glasses and molecular dynamics calculations [J]. *Materials Transactions*, 2007, 48(11): 2923–2927.
- [33] GIWA A M, AITKEN Z H, LIAW P K, ZHANG Y W, GREER J R. Effect of temperature on small-scale deformation of individual face centered-cubic and body-centered-cubic phases of an $\text{Al}_{0.7}\text{CoCrFeNi}$ high-entropy alloy [J]. *Materials & Design*, 2020, 191: 108611.
- [34] LANDAU L D, LIFSHITZ E M. *Theory of elasticity* [M]. New York: Pergamon, 1986.

不同加载速率下氧化铝纳米线弯曲力学行为的分子动力学研究

贺宇骁¹, 马彬²

1. 清华大学 材料科学与工程学院, 北京 100084;
2. 桂林电子科技大学 建筑与交通工程学院, 桂林 541004

摘要: 采用 LAMMPS 软件建立弯曲加载下 α -Al₂O₃ 纳米线的分子动力学(MD)模型, 计算并分析不同加载速率下 α -Al₂O₃ 纳米线的原子应力和应变, 揭示加载速率对其弯曲力学行为的影响规律。研究表明: α -Al₂O₃ 纳米线在不同加载速率下的最大表面应力-转角曲线均可分为弹性变形、塑性变形和破坏 3 个阶段, 弹性极限点可通过加、卸载循环下的曲线对称性来确定; 加载速率对 α -Al₂O₃ 纳米线的塑性变形影响很大, 但对弹性模量影响较小; 当加载速率增加时, 塑性变形阶段缩短, 材料更易发生脆性断裂, 且弹性极限和强度极限(由直接和间接 MD 法确定)更加接近。MD 模拟结果与改进的弯曲环路试验结果吻合良好, 从而验证分子动力学建模和计算方法的有效性。直接 MD 法是确定在任意加载速率下(无论发生脆性还是韧性断裂)纳米晶须弹性极限和强度极限的有效方法。

关键词: 氧化铝纳米线; 弯曲性能; 加载速率; 弹性极限; 强度极限; 分子动力学

(Edited by Bing YANG)